Resistive switching mechanism of TiO_2 thin films grown by atomic-layer deposition

B. J. Choi, D. S. Jeong, and S. K. Kim
School of Materials Science and Engineering and Inter-university Semiconductor Research Center, Seoul National University, Seoul 151-742, Korea

C. Rohde
School of Materials Science and Engineering and Inter-university Semiconductor Research Center, Seoul National University, Seoul 151-742, Korea and Institute of Electronic Materials, Institut für Festköperforschung (IFF), Forschungszentrum, 52425 Jülich, Germany

S. Choi, J. H. Oh, H. J. Kim, and C. S. Hwang[a)]
School of Materials Science and Engineering and Inter-university Semiconductor Research Center, Seoul National University, Seoul 151-742, Korea

K. Szot and R. Waser
Institute of Electronic Materials, Institut für Festkörperforschung (IFF), Forschungszentrum, 52425 Jülich, Germany

B. Reichenberg
Institute of Electronic Materials, Institut für Festkörperforschung (IFF), Forschungszentrum, 52425 Jülich, Germany and Aixacct Gesellschaft mit Beschränkter Haftung (GMBH), Aachen 52068, Germany

S. Tiedke
Aixacct Gesellschaft mit Beschränkter Haftung (GMBH), Aachen 52068, Germany

(Received 27 January 2005; accepted 17 June 2005; published online 15 August 2005)

The resistive switching mechanism of 20- to 57-nm-thick TiO_2 thin films grown by atomic-layer deposition was studied by current-voltage measurements and conductive atomic force microscopy. Electric pulse-induced resistance switching was repetitively (> a few hundred times) observed with a resistance ratio $\geqslant 10^2$. Both the low- and high-resistance states showed linear log current versus log voltage graphs with a slope of 1 in the low-voltage region where switching did not occur. The thermal stability of both conduction states was also studied. Atomic force microscopy studies under atmosphere and high-vacuum conditions showed that resistance switching is closely related to the formation and elimination of conducting spots. The conducting spots of the low-resistance state have a few tens times higher conductivity than those of the high-resistance state and their density is also a few tens times higher which results in a $\sim 10^3$ times larger overall conductivity. An interesting finding was that the area where the conducting spots do not exist shows a few times different resistance between the low- and high-resistance state films. It is believed that this resistance change is due to the difference in point defect density that was generated by the applied bias field. The point defects possibly align to form tiny conducting filaments in the high-resistance state and these tiny conducting filaments gather together to form stronger and more conducting filaments during the transition to the low-resistance state. © *2005 American Institute of Physics*.
[DOI: 10.1063/1.2001146]

I. INTRODUCTION

The resistance switching behavior of several oxide and chalcogenide thin-film materials recently attracts great interest for the application in nonvolatile memory elements in semiconductor memory devices.[1] Apart from random access memories using phase change material (PcRAM) where a large reset current hinders high-density integration, the resistive switching RAM (ReRAM) without a phase change of the material offers the possibility of very high density integration and lower power operation. In addition, the resistance-change-based RAMs are believed to be more free from the inherent scaling problem than the capacitance-based RAMs, such as dynamic RAM (DRAM) and ferroelectric RAM (FeRAM).[1,2] There have been many different suggestions for materials showing resistance switching by electric pulses without phase change.[3–6] Here, "phase change" means the complete change in the phases of the switching materials between amorphous (usually high-resistance state) and crystalline (usually low-resistance state) by a heat pulse. The heat pulses are usually produced by electric current flow in the solid-state device. Colossal magnetoresistive switching material, such as $(Pr,Ca)MnO_3$,[3,4] systems with electromigration of metallic ions into a nonconducting chalcogenide glass material, such as the $Ag–Ge_xTe_y$ system,[5] and electric pulse-induced threshold switching in other chalcogenide glass materials, such as the $Ge_2Sb_2Te_5$ system,[6] are some examples for ReRAM devices. Bulk and thin films of transition-metal

[a)]Electronic mail: cheolsh@plaza.snu.ac.kr

oxides, such as NiO,[2,7] TiO_2,[8] $SrZrO_3$,[9] and even SiO_2,[10] are also known to show a resistive switching behavior. However, the switching mechanisms are still unclear although the switching behavior itself has been clearly observed and many physical and theoretical models, including band bending by charge trapping[11] and the change in the oxidation state of the cations,[12] have been suggested. One of the reasons for such an unknown mechanism is the poorly defined material quality in earlier times.

The other factor that has to be considered for the application of resistive switching material into RAMs is the physical thickness of the films. As the device size scales down to the sub-100-nm region, the film thickness must be less than a few hundred nanometers or otherwise the device fabrication becomes difficult. Film thickness scaling is also important for guaranteeing low-voltage (<1 V) operation of the device which is essential for mobile applications where nonvolatile memories are mostly adopted.

Therefore, this study investigated the resistive switching behavior of atomic-layer-deposited (ALD) TiO_2 films with a well-controlled quality which was obtained by the inherent nature of the fabrication process, i.e. the self-limiting property of the ALD process. The film thickness was between 20 and 57 nm which is appropriate for highly integrated device fabrication as well as low-voltage operation.

II. EXPERIMENTAL PROCEDURES

TiO_2 thin films were grown by ALD using $Ti(OC_3H_7)_4$ and O_3 as precursor and oxidant, respectively, at a wafer temperature of 250 °C on a $Ru/SiO_2/Si$ wafer. Ru thin films of 50-nm thickness were deposited by sputtering. The TiO_2 film thickness was changed from 20 to 57 nm by changing the number of deposition cycles. The grown films have a polycrystalline microstructure with a rutile crystal structure. The TiO_2 films have a dielectric constant of approximately 70 and good insulating properties. Details of the film growth process and film characterization results were previously reported.[13] After TiO_2 film deposition, Pt and Al top electrodes with a diameter of approximately 300 mm were fabricated by electron-beam evaporation through a metal shadow mask. During the electrical measurements of resistive switching, the Ru bottom electrode was grounded and the bias voltage was applied to the top electrode, In the following, the electrical measurements using these pad-shaped electrodes are called pad current-voltage (*I-V*) measurements. The $Pt/TiO_2/Ru$ capacitors showed the resistive switching behavior irrespective of the bias polarity on the Pt top electrode. However, the $Al/TiO_2/Ru$ capacitors showed the switching behavior only when positive bias was applied to the Al top electrode. The reason for this electrode-dependent bi- or unipolar switching behavior seems to be the oxygen permeation through the top electrode, and more details will be reported separately. Meanwhile, the switching behavior of the $Al/TiO_2/Ru$ capacitors under positive bias was almost identical to that of the $Pt/TiO_2/Ru$ capacitors. Resistive switching was tested using the Hewlett Packard 4155 semiconductor parameter analyzer or the Aixacct TF 2000 analyzer with ferroelectric module at measurement temperatures ranging from 30 to 110 °C.

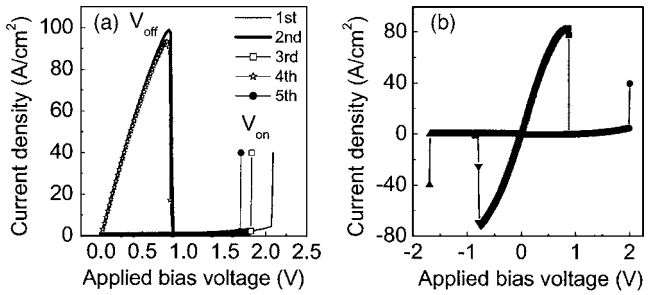

FIG. 1. (a) Typical current density vs voltage (*J-V*) curve of a 57-nm-thick TiO_2 film with Pt electrodes. (b) *J-V* curve under positive and negative biases.

Local conductivity measurements were made using two atomic force microscopy (AFM) systems with conductive tips (CAFM) at room temperature. The two AFM systems, operated under atmospheric pressure (SEIKO, SPA400, Au-coated tip) and high vacuum (10^{-7} Torr) (JEOL JSPM 4210, Ptlr-coated tip), respectively, were used to investigate the difference between the conduction properties of the high- and low-resistance states. For the CAFM measurements, some of the $Al/TiO_2/Ru$ capacitors were switched either to the high- or low-resistance state by applying a proper bias voltage and the Al top electrodes were etched away by a nitric acid solution. Then the film surface morphology and local conductivity of TiO_2 films in the high- and low-resistance states below the Al electrodes were investigated. During the CAFM measurements, the bottom Ru electrode was grounded.

III. RESULTS AND DISCUSSIONS

A. Macroscopic results from the pad *I-V* measurements

The resistance per unit area (1 cm^2) of the as-deposited films was approximately 10^9 Ω in the voltage region from -1 to 1 V, which is the intended device operation voltage range, and the films did not show any resistive switching behavior. Therefore, a rather high bias voltage (2.0–2.5 V for the 57-nm-thick TiO_2 sample) was applied to the capacitors in order to make the films less resistive ($\sim 10^6$ Ω at 1 V). During this initial bias application process, the leakage current suddenly increased (soft breakdown) to a certain limiting value (a few tens milliampere). If the suddenly increased current was too high (>0.07 A) the capacitors were hard broken down and became useless. Therefore, setting a proper current limit (current compliance) was crucial.

Figure 1(a) shows a typical current density versus voltage (*J-V*) curve of a 57-nm-thick TiO_2 film with Pt electrodes. After the initial soft breakdown (first measurement), the film remains in the low-resistance state (LRS) so that *J* under both positive and negative bias shows a high value (50 A/cm^2 at 0.5 V). With increasing voltage the current density increases and then suddenly drops to a very low value at a certain voltage (V_{off}) during the second measurement. Then, the third *J-V* measurement shows the high-

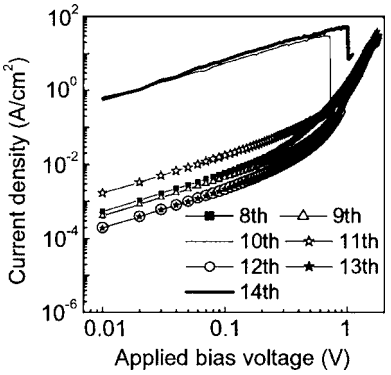

FIG. 2. *J-V* curves of a 57-nm-thick film plotted in logarithmic scale.

resistance state (HRS) where J at 0.5 V is approximately 10^{-2} A/cm^2. Figure 1(b) shows that switching occurs under both polarities. For further increase in V, typically up to 1.5 V, HRS is maintained but then at the higher voltage (V_{on}) J suddenly increases to the current compliance value again and LRS is recovered. V_{off} is always smaller than V_{on}. This is how resistance switching was observed. When V is limited to far less than V_{off}, LRS and HRS were not disturbed up to at least a few hundreds readings and the data retention time at room temperature is more than a few hundreds hours. Resistive switching was also repeatedly observed at least a few hundreds times.

In order to understand the leakage conduction mechanism in the LRS and HRS, the *J-V* curves of the 57-nm-thick film are plotted on a logarithmic scale, as shown in Fig. 2. Here, out of 20 measurements the results from the 8th to the 14th sweep (positive bias sweeps) are shown in the low-voltage ($<$1.1 V) region. It can be clearly observed that the LRS (upper graphs) shows linear log J vs log V graphs with a slope of 1 up to V_{off}, which is 0.8–1.0 V in Fig. 2, whereas the HRS (lower graphs) shows linear behavior only in the low-voltage region ($<\sim$0.5 V). It has to be noted that the linear *J-V* curve does not necessarily mean that the conduction is "Ohmic." The current density of the HRS shows an almost exponential increase with V in the high-voltage region ($>$0.5 V) until V_{on}, above which a super exponential increase in J was observed (not included in Fig. 2). It should be noted that there is a subtle difference between the switching from LRS to HRS and from HRS to LRS. The LRS retains its conductivity immediately up to V_{off} before switching occurs but the HRS has a conductivity similar to the LRS before switching to the LRS. This behavior gives some clue to understanding the nature of resistance switching.

In Fig. 2, different bias conditions were chosen to show the switching and sensing processes. For example, during the eighth measurement, the sample was in the HRS and the voltage was limited to 1.1 V so that switching to the LRS did not occur although the current density already deviated from the linear behavior in the voltage region of $0.5\ \text{V} < V < 1.1$ V. The ninth measurement shows an almost identical *J-V* curve in the V region $<$1.1 V, but this time the voltage was increased up to 2 V so that the sample switched to LRS and the tenth measurement shows a high J level.

From the *J-V* measurement results given above, the following can be assumed for the switching phenomenon in these TiO_2 films. First, it has to be noted that the contact between the TiO_2 film, generally being regarded as an n-type wide-band-gap semiconductor due to the oxygen vacancies, and the metals such as Pt and Ru, which have a large work function (5.5 and 5.1 eV, respectively), is blocking so that a linear electrical conduction behavior in the low-voltage region cannot be observed. Therefore, the occurrence of linear conduction in both states suggests that there is a certain structural change in the TiO_2 film that can create some linear and highly conducting paths.

One of the probable models for the formation of linear conducting paths is the formation of conducting filaments throughout the insulating film.[14] The conducting filament is one of the specific forms of extended defects in insulating ionic crystals.[15] Since the conducting filaments are of metallic or metal-like nature, linear conduction can be observed in the *J-V* measurements once they extended throughout the TiO_2 film.

Szot *et al.* showed that there are many extended defects, especially along the grain boundaries of polycrystalline samples, in Ti-containing ionic crystals, such as TiO_2, $SrTiO_3$, and $PbTiO_3$ using conductive AFM measurements.[15] The extended defects show a local conductivity more than a few orders of magnitude higher than the rest of the insulating material. They also found that even single crystals could show the extended defects especially under a local high electric field applied by the AFM tip. This may be due to the relatively easy transition of the oxidation states of Ti ions in the ionic crystals. The Ti–O binary phase diagram[16] shows that there are many intermediate phases (Ti_nO_{2n-1}, so-called Magnelli phases in addition to Ti_2O, TiO, Ti_2O_3, Ti_3O_5, and TiO_2). When ionic oxide crystals, such as TiO_2, are reduced (oxygen vacancies are formed), conduction electrons are simultaneously released in order to maintain the total charge balance. These conduction electrons can be rather localized around the reduced Ti ions centers (or oxygen vacancies) due to the weak Coulombic interaction.

When the bias voltage was applied to the top electrodes, the oxygen ions in the TiO_2 thin film were influenced by the high electric field (a few hundreds kV/cm) and began to move. There is few evidence for the oxygen ion movement under a high electric field even at room temperature. The thin-film Pt electrode is well known to have a high oxygen mobility in it[17] so that the release of oxygen ions from TiO_2 to the atmosphere or the incorporation of the oxygen ions from the atmosphere in the TiO_2/Pt interface must be fast and active. This is basically due to the nonoxidizing property of Pt which guarantees easy movement of oxygen ions or atoms along grain boundaries. In contrast to this, Al oxidizes so easily that the permeation of oxygen through the Al thin-film electrode is almost impossible at room temperature. Now, it has to be remembered that resistance switching with an Al top electrode was only possible under positive bias. Under this condition, O^{2-} ions in the TiO_2 thin film were pulled into the Al electrode and oxidized it. It was observed that the Al electrode was actually oxidized during positive bias application but no change in the physical state of the Al

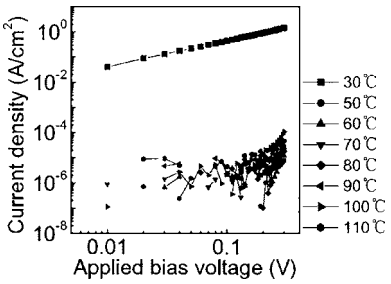

FIG. 3. Variation of the *J-V* curve of the high-resistance state with the measurement temperature in the voltage region with linear conduction.

electrode was observed when a negative bias was applied. This was confirmed by wet-etching experiments; when an excessively high positive bias with a long duration was applied to the Al electrode (actually oxidized Al electrode), it did not dissolve into the nitric acid whereas the mildly positively biased, negatively biased, and nonbiased electrodes completely dissolved into the same acid.

The change in the oxidation state of Ti ions in $SrTiO_3$ single crystals by an applied electric field (a few tens of kV/cm) at elevated temperatures (~500 °C) has been reported by He *et al.*[18] It seems that the excessively high electric field in the thin-film experiments made the oxygen ions move even at room temperature.

Therefore, it is believed that the changes in the chemical state of the TiO_2 films during the resistance switching measurements take place as follows. During the first application of a high positive voltage to the as-deposited samples, a large number of O^{2-} ions are pulled into the electrode and oxygen vacancies are formed. When negative bias is applied, the O^{2-} ions are pushed away from the top electrode interface and maybe diffuse out to the atmosphere along the top electrode/TiO_2 interface. For a Pt electrode this interface diffusion might be fast enough, but for an Al electrode the strong interaction between Al and oxygen ions may make the interface diffusion difficult.

At a certain high voltage, such generated defects might align to form filamentlike throughout the film, forming a local conducting path. The filament formation might be triggered at a certain point (local protrusion or defective site) at the elecrode/TiO_2 interface. Once the paths are formed the current flow concentrates on these local paths and the conducting paths grow very fast due to local heating by the concentrated current flow. This corresponds to the switching from HRS to LRS. The destruction of the filaments (switching from LRS to HRS) is believed to be accomplished by the thermal rupture of the filaments, i.e., by the heat produced by the large current flow.

Although the nature of the conducting filaments is not clearly known at this moment, it is clear that the formation and destruction of the filaments have a close relationship with local heating effects as shown below.

Figure 3 shows the variation of the *J-V* curve of the HRS with the measurement temperature in the voltage region with linear conduction. These measurements were actually performed to confirm the metallic conduction nature of the state (increasing resistance with increasing temperature). However, the results are very contradictory to the expectation; when the measurement temperature increases to only 50 °C, the conductivity drops by more than four orders of magnitude in the whole voltage region, and shows a scattered leakage behavior with increasing temperature. The scattered *J* in such a low-voltage region is due to measurement noises. It is believed that most of the conducting filaments that maintain the low conductivity in the HRS are destroyed by the heating of the samples and the sample looses its electrical conductivity.

The LRS conductivity was also influenced by the measurement temperature but it was more stable than the HRS, as shown in Fig. 4. Figures 4(a)–4(c) show the *J-V* curves of the LRS sample at measurement temperatures of 50, 70, and 110 °C, respectively. It can be observed that the high conductivity was stably maintained up to 90 °C (data not included in Fig. 4) but began to be disturbed at 110 °C. This means that the difference between the conductivities of the LRS and HRS is not simply due to the difference in the number of conducting filaments. The filaments themselves in the LRS and HRS appear to be different; filaments in the LRS are more immune to thermal disturbance and more conducting than those in the HRS. It is not believed that the types of the defects that form the filaments in the LRS and HRS are different, but the degree of correlation between the defects is different. This was confirmed by the CAFM results as shown later. The difference in the thermal stabilities of the LRS and HRS is also observed in the retention behavior of the two samples, as shown in Fig. 5. Figure 5 shows that the resistance of both states, LRS and HRS, increases with time even at room temperature. The increase rate of the HRS is 5.2 times faster than that of the LRS, again suggesting that the conducting filaments of the LRS are more immune to thermal disturbance than those of the HRS even at room temperature. Therefore, investigation of the conducting spots on the film surface under the Al electrode was performed using a CAFM.

Before, the results from the nanoscale investigations are discussed, and the TiO_2 film thickness-dependent resistance is described. Figures 6(a) and 6(b) show the variation in the resistance of the HRS and LRS, respectively, as a function of

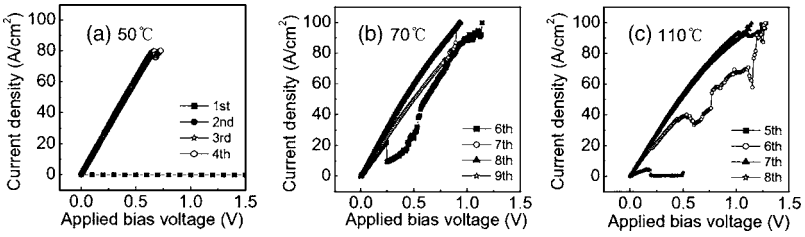

FIG. 4. *J-V* curves of samples in the low-resistance state at measurement temperatures of (a) 50, (b) 70, and (c) 110 °C.

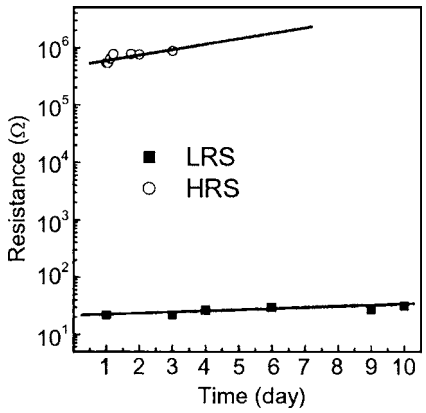

FIG. 5. Retention behavior of samples in the low- and high-resistance states, respectively. The resistance of both states increases with time even at room temperature.

the TiO_2 film thickness. Here, the resistance was measured at 0.5 V. If the conduction mechanism is strictly "Ohmic" the resistance should be linearly dependent on the film thickness. The LRS and HRS resistances indeed increase with film thickness. However, the HRS shows a superlinear dependency (film thickness increases by 2.85 times but the resistance increases by almost 10 times) whereas the LRS shows a sublinear dependency (film thickness increases by 2.85 times but the resistance increases by only 1.2 times). This suggests that the electrical conduction is not simply mediated by purely Ohmic conducting filaments. The interface between the filaments and the electrodes may still play some role. The x-ray photoelectron spectroscopy study (XPS) of the LRS and HRS TiO_2 films did not show any difference in the binding status of the Ti and oxygen ions. This might be due to the small surface area ratio of the conducting spots on both samples.

B. Nanoscale investigation using conductive atomic force microscopy

CAFM appears to be one of the best experimental tools to investigate the local conductivity of dielectric thin films considering the restricted interaction area of the tip and film surface. However, if the conducting spot area is comparable or smaller than the effective area of the tip-surface interaction, the interpretation of the measurement results becomes complicated due to convolution- and multiple-measurement effects. These effects will be explained in detail later. Furthermore, the effective tip area that is responsible for the electrical contact with the surface depends on many parameters, such as the tip material, radius, force, contamination, etc., so that it is usually difficult to define the precise tip-surface interaction area. Therefore, the determination of the absolute area of the conduction spots was not pursued but the relative area ratio of the conducting spots in the LRS and HRS was investigated. The sharp shape of the tip may enhance the local electric field so that the current density measured by the CAFM could be larger than the current density from the pad *I-V* results. Therefore, quantitative understanding of the CAFM results and their comparison with the pad *I-V* results required a careful consideration and several reasonable assumptions on the interaction between the tip and film surface should be made. However, from these results, the differences between the properties of the conducting spots of the two states were better understood. For this purpose, two CAFMs operated under high vacuum (HVAFM) and atmospheric pressure (APAFM), which are believed to have different tip-surface interactions, were used in this study.

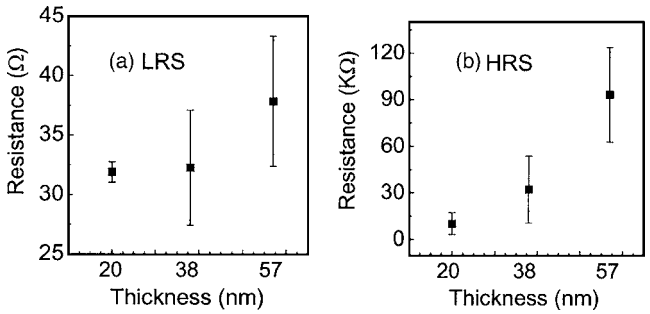

FIG. 6. Variation in the resistance of the (a) low- and (b) high-resistance states as a function of the TiO_2 film thickness measured at 0.5 V.

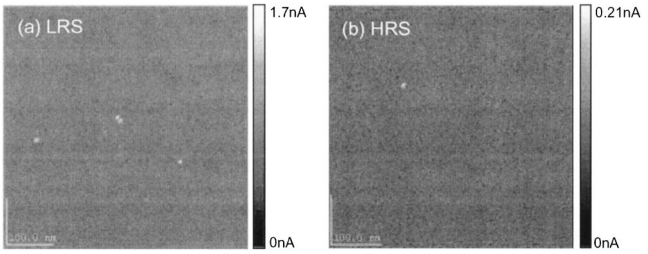

FIG. 7. Conductivity mapping results of the (a) low- and (b) high-resistance state TiO_2 films, using HVAFM. The bright spots represent the conducting spots.

Figures 7(a) and 7(b) show the conductivity mapping results of the LRS and HRS TiO_2 films, respectively, using HVAFM where the bright spots represent conducting spots. Here, +1 V was applied to the tip during the measurements. The AFM indeed shows that there are many conducting spots on the TiO_2 films with a higher density in the LRS. Although the presence of the conducting spots qualitatively confirms the filament model for resistive switching, a quantitative comparison of the CAFM data with the pad *I-V* measurement results shows many discrepancies.

First, the total current densities measured by the pad *I-V* and HVAFM are compared. The pad *I-V* measurements show that the LRS and HRS have current densities 48 and 0.038 A cm^{-2} at +1 V, respectively, which correspond to a current ratio of approximately 1300. The total current per area at the same voltage from the HVAFM can be obtained by statistically treating the data shown in Figs. 7(a) and 7(b).

Figures 8(a) and 8(b) show the distribution of the number of conducting spots as a function of the current at each spot for the LRS and HRS, respectively. The integrated area of the two graphs corresponds to the total current measured by HVAFM. A few notable facts were found; first, the total current densities from the HVAFM are 1250 and 200 A cm^{-2}, for the LRS and HRS, respectively. Therefore, the current density ratio is only 6.25. This is a much smaller value than that of the pad *I-V* results. Second, the total cur-

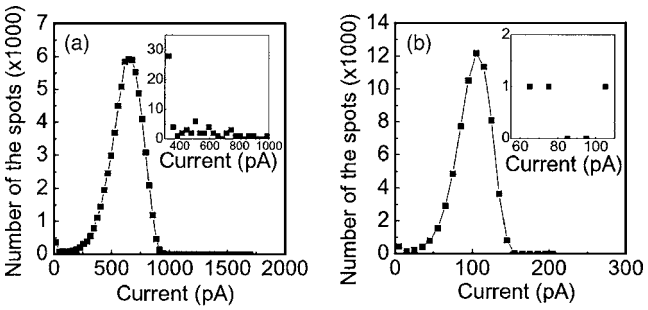

FIG. 8. Distribution of the number of conducting spots as a function of the current at each spot for the (a) low- and (b) high-resistance states measured by HVAFM. The inset figures show the rectified distributions after subtracting the most probable current.

rent density of the HVAFM is 26 and 5263 times higher than that of the pad *I-V* results for the LRS and HRS, respectively. In order to understand such a large discrepancy, the HVAFM data were carefully investigated. Figures 8(a) and 8(b) show that the most probable current values per AFM measurement, where the nominal contact area per measurement is $\sim 50\ \mathrm{nm}^2$ $[(1800\ \mathrm{nm}/256)^2]$, are approximately 620 and 100 pA for the LRS and HRS, respectively. These values correspond to a current density of $1240\ \mathrm{A\,cm}^{-2}$ $(620\ \mathrm{pA}/50\ \mathrm{nm}^2)$ and $200\ \mathrm{A\,cm}^{-2}$ $(100\ \mathrm{pA}/50\ \mathrm{nm}^2)$ for the LRS and HRS, respectively, which are much larger than the pad *I-V* result. It is believed that the most probable current value corresponds to the current through the nonconducting parts of the films because most of the area remains insulating [Figs. 7(a) and 7(b)]. Therefore, it is believed that the sharp shape of the CAFM tip largely enhanced the local electric field and thus thermionic emission or tunneling occurred at the tip-surface interface even at 1 V. It has to be noted that the pad *I-V* measurement showed that the current flow is almost linearly dependent on *V*, suggesting that most of the current flows only through the conducting spots. The nonlinear conduction characteristics of the HVAFM measurement are actually confirmed by its *I-V* curves shown in Fig. 9 which show the $\log I$ vs $\log V$ curves of a typical nonconducting and conducting spot of the LRS and a conducting spot of the HRS. The slopes of the graphs in the high-voltage region

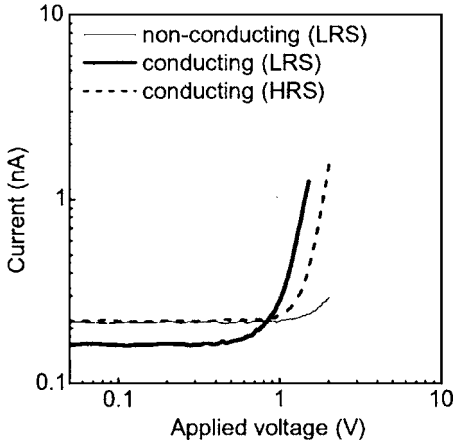

FIG. 9. *I-V* curve in logarithmic scale of a typical nonconducting, a conducting spot of the low-resistance state, and a conducting spot of the high-resistance state.

$(>0.8\ \mathrm{V})$ are approximately four, suggesting that the current flows by a leakage mechanism such as Schottky emission or tunneling. The study on the details of the conduction mechanism will be a topic of next research. Therefore, it can be understood that the much larger total current density of the HVAFM compared to the pad *I-V* results in both states, LRS and HRS, is due to the large leakage current through the nonconducting area owing to the sharp tip-shape-induced locally enhanced electric field. It is interesting to note that the HVAFM *I-V* characteristics of the conducting spots are not linear either. This suggests the following fact. When the HVAFM tip contacts the conducting spots, the tip-surface contact area is much larger than that of the cross-section area of each conducting filament so that a large portion of the current still flows through the nonconducting area around the filaments. Therefore, the current through the nonconducting part should be subtracted from the total current that was measured from the area that contains the conducting filaments in order to compare the HVAFM results to the pad *I-V* results.

When the distributions of the measured current values at each point, shown in Figs. 8(a) and 8(b), were carefully investigated, it was found that the number of spots that have current values similar to the most probable one drops down abruptly and there are only a few tens and a few spots which show distinctively larger current values for the LRS and HRS, respectively. These are believed to correspond to the conducting spots. Their number distribution over the current value after subtracting the most probable current at the respective state is shown in the inset figures of Figs. 8(a) and 8(b). Now, the current values obtained from the integration of the inset graphs should correspond to the total current only through the conducting filaments in the LRS and HRS. These total current densities are 6.1. and $0.0076\ \mathrm{A\,cm}^{-2}$ for the LRS and HRS, respectively. The total current-density ratio is approximately 800 which is quite close to the ratio from the pad *I-V* measurements (1300). However, the current densities are almost eight $(48\ \mathrm{A\,cm}^{-2}$ vs $6.1\ \mathrm{A\,cm}^{-2})$ and five $(0.038\ \mathrm{A\,cm}^{-2}$ vs $0.0076\ \mathrm{A\,cm}^{-2})$ times smaller than those from the pad *I-V* results at their respective states. This can be understood from the fact that the conducting filament ends that were exposed to the wet-etching solution for the electrode removal or to air after the electrode removal might be contaminated, which results in a relatively poor electrical contact between the HVAFM tip and the filaments. However, the quantitative agreement between the current-density ratio of the HVAFM and the pad *I-V* results strongly suggests that resistive switching of TiO_2 films has a close relationship with the formation and modification of conducting filaments by an applied electrical field. The inset figures of Figs. 8(a) and 8(b) show that the conducting filament density ratio between the LRS and HRS is approximately 33. Therefore, the conductivity ratio (k) of the filaments of the LRS and HRS is approximately 24.3 (800/33).

The third point that has to be noted from the HVAFM is the difference of the most probable current values of the LRS and HRS. As mentioned earlier, these values represent the current values through the area where no conducting filaments were formed. However, they are still almost six times different, suggesting that even the nonconducting area of the

LRS is more conducting than that of the HRS. The higher emission or tunneling leakage current through an insulating film implies that the point defect density is higher.[19,20] This suggests the following mechanism for resistive switching; when a high voltage is applied to the TiO_2 film, many point defects (probably oxygen vacancies) are formed and at a certain voltage (V_{on}) these defects gather together to form the extended defects (conducting filaments). It is also considered that several noncomplete filaments (not extended throughout the whole film thickness) are formed in the nonconducting area and that they contribute to the leakage current.

Spectroscopic analysis using XPS of the films with two states did not show any difference as discussed earlier. It was noted that the point defect density as high as 10^{19} cm^{-3}, which is a high enough value to influence the resistances of the area without conducting filaments, is still less than 1% of the total ionic concentration of TiO_2. This may constitute the reason for no observable difference in XPS. Therefore, unfortunately the assumption regarding the point defects cannot be confirmed by any spectroscopic means at this moment.

This understanding is not only important for the understanding of the switching mechanism but also for the practical application of the material to memory devices. It was noted from the HVAFM results shown in Figs. 7 and 8 that only a few tens of filaments are formed in a few μm^2. Therefore, it can be easily imagined that when memory devices with a feature size of <100 nm are fabricated, most of the switching elements do not contain conducting filaments. Therefore, the resistance switching must depend on the resistance change of the nonconducting area and not on the formation and destruction of the filaments. Then the switching signal margin may not be ~ 1000 but ~ 5, which is still big enough for a stable memory operation.

The current measurements using APAFM enabled a better understanding of the nature of the conducting filaments and the resistive switching behavior of TiO_2 films. It is believed that the APAFM worked with a much larger tip-surface interaction area due to more and larger contaminants on the tip and film surface. If the effective interaction area is larger than the nominal probing area of each measurement $[(500\ \text{nm}/128)^2 \sim 15\ \text{nm}^2]$, the current flow through each measurement area multiply contributes to the total current (multiple effect). Similarly, if the distance between the conducting spots (filaments) is smaller than the effective contact diameter (d_{eff}), one measurement convolutes many filaments. These effects are schematically shown in Fig. 10. They were not considered for the HVAFM since the effective contact area was not believed to be significantly larger than the nominal contact area and the effective contact diameter was smaller than the distance between the filaments. Therefore, the APAFM results may not be useful to investigate the conducting filaments that were formed by the pad *I-V* tests. However, as shown below, the APAFM results were found to be useful to understand the dynamics or change of the filaments during voltage application.

Figures 11(a) and 11(b) and show the distribution of the number of conducting spots as a function of the current at each spot for the LRS and HRS, respectively, using APAFM. As done for the HVAFM case, the total current density and most probable current value are calculated using the data in Fig. 11 and are 16 400 and 6600 A cm^{-2} and 1000 and 400 pA for the LRS and HRS, respectively. The total current density ratio is approximately 2.5 which may result from the field-enhancement, multiple, and convolution effects. First, in order to exclude the leakage current through the nonconducting area due to the field-enhancement effect, the most probable current was subtracted from the current data in Fig. 11 and the high current tail parts of the graphs are shown in the inset figures in Fig. 11, as done for the HVAFM case. Now, the current values calculated by the integration of the inset graphs are 2300 and 23.6 A cm^{-2} for the LRS and HRS, respectively, and the ratio is approximately 100. This value is still much smaller than that from the pad *I-V* (1300) and HVAFM (800) results. The current value itself is 48 (2300/48) and 620 (23.6/0.038) times larger than that from the pad *I-V* results for the LRS and HRS, respectively. It should be noted that such large current values were obtained even after the subtraction of the background leakage current through the nonconducting area around the filaments. The $\log I$-$\log V$ curves of the APAFM also show a slope >1 (~ 6), suggesting that the field-enhancement effect is also occurring in this case. Therefore, the reason for this discrepancy must be found from the multiple and convolution effects, considering the larger tip-surface interaction area.

In order to confirm the involvement of these effects, the most probable current value is carefully considered. If the most probable current flows through one nominal measurement area, then the current densities are approximately 6700 A cm^{-2} (1000 pA/15 nm^{-2}) and 2700 A cm^{-2}

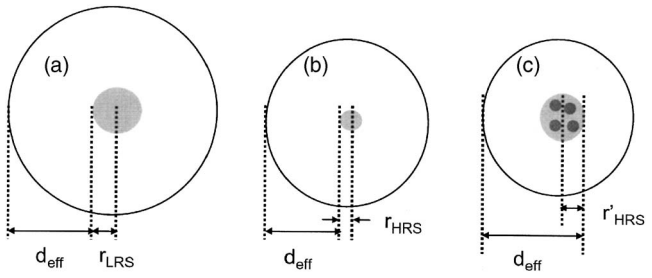

FIG. 10. Schematic of the multiple effect for the (a) 1ow-resistive state and (b) high-resistive state. (c) shows a schematic of the convolution effect for the high-resistance state considering the larger tip-surface interaction area in the case of APAFM.

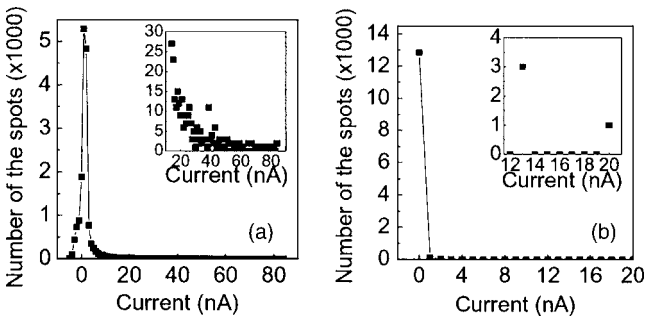

FIG. 11. Distribution of the number of conducting spots as a function of the current at each spot for the (a) low- and (b) high-resistance states measured by APAFM. The inset figures show the rectified distributions afer subtracting the most probable current.

(400 pA/15 nm^{-2}) for the LRS and HRS, respectively, which are 5.4 and 13.5 times higher than that of the HVAFM. Therefore, in most measurements of the APAFM, the current flow through a much larger area and the total current are overestimated as many times as the ratio of the effective contact area to the nominal measurement area.

The current overestimation by the multiple effect can be rather easily formulated into equations by considering the following fact. The conducting spots are assumed to have a circular cross section with a radius of r_{LRS} for the LRS. It can be assumed that the electrical contact between the tip and the conducting spot is made whenever the tip gets into the circular area having a radius of $(r_{LRS}+d_{eff})$, see Fig. 10(a). For the pad *I-V* measurements the current flows only through the conducting filaments and no multiple and convolution effects are involved. Therefore, the measured current ratios between the pad *I-V* and APAFM of the LRS (I_{LRS}^{P}/I_{LRS}^{A}) and HRS (I_{HRS}^{P}/I_{HRS}^{A}) are given as Eqs. (1) and (2), respectively, if only the multiple effect is involved;

$$\frac{r_{LRS}^{2}}{(r_{LRS}+d_{eff})^{2}}=\frac{I_{LRS}^{P}}{I_{LRS}^{A}}. \tag{1}$$

$$\frac{r_{HRS}^{2}}{(r_{HRS}+d_{eff})^{2}}=\frac{I_{HRS}^{P}}{I_{HRS}^{A}}. \tag{2}$$

Here, it is assumed that the distance between the filaments is much larger than the effective tip diameter so that no convolution effects are considered and no additional filaments are produced during the measurements.

The I_{LRS}^{P}/I_{LRS}^{A} and I_{HRS}^{P}/I_{HRS}^{A} are 48^{-1} and 620^{-1} so that r_{LRS}/r_{HRS} is calculated to be approximately 4 (area ratio of 16) using Eqs. (1) and (2). If the specific conductivities of the filaments in LRS and HRS (conductivity per unit cross-section area of the filament) are the same, the conductivity ratio of the filaments of the two states must be 16. In order to confirm the validity of this number the following comparison is made.

The inset figures in Fig. 11 show that the number ratio of the highly conducting spots (containing the filaments) is approximately 40 so that the average conductivity ratio from the APAFM (k') of each of the conducting spots in LRS and HRS should be approximately 2.5 (100/40). It has to be noted that the average conductivity ratio from the HVAFM (k) should not be used for this comparison because the APAFM measurement itself modifies the density and distribution of the filaments as shown later.

This suggests that the specific conductivity of the filaments in the HRS should be larger than that of the LRS if the area ratio is 16 as discussed above. However, this looks unreasonable considering the better thermal stability (shown in Figs. 3 and 4) of the LRS filaments. It can be reasonably assumed that the filaments are formed by the alignment and connection of point defects during applied bias. Therefore, a different model for the distribution of the conducting filaments is necessary to explain the APAFM results.

Before this new model is discussed, the viability of the APAFM current distribution shown in the inset figures of Fig. 11 is confirmed by the following. If the number and conductivity ratios of the conducting filaments in both states are known, the product of these two ratios must correspond to the current-density ratio from the pad *I-V* measurement. Now, for the APAFM measurements, the number ratio is 40 [161 for LRS and 4 for HRS from the inset figures of Figs. 11(a) and 11(b)]. The conductivity ratio (k) of the filaments in the two states was 24.3 obtained from the HVAFM. Therefore, the product is 960 which is close to the pad *I-V* result (1300), suggesting the valid estimation of the number of conducting spots shown in Fig. 11 for the APAFM. It should be noted that k, not k', was used here. This is done because the conductivity of one filament in the HRS was increased during the APAFM measurements due to the large current flow compared to the HVAFM, as shown below, and thus k' does not represent the original conductivity ratio of the two states. However, the pad *I-V* current ratio must be derived from the product of the number ratio and the original conductivity ratio of the filaments of the two states.

It was found that the conduction states of the films were influenced during the APAFM measurements; more filaments were generated due to the excessive current flow during the APAFM measurements. This could be confirmed by the repeated APAFM measurements of the same area; in the second measurement the conductivity of the film was increased. This change was substantial in the case of HRS but LRS showed a relatively small change. Therefore, it can be assumed that the filaments of the LRS are negligibly influenced by the APAFM measurements. In addition, they are sufficiently distant from each other considering the HVAFM results (Fig. 7). Therefore, only multiple effects should be considered for the LRS film in the APAFM measurement, and, thus, Eq. (1) is still valid for the LRS.

Now, the correlation between the pad *I-V* and APAFM results of the HRS becomes rather complicated due to the generation of additional filaments during the APAFM measurements. However, it was noted that the additional filaments must be generated near the preexisting filament due to local heating by the current flow through the preexisting filament. Therefore, it can be reasonably assumed that the current contributing to each APAFM measurement for HRS flows through n filaments with a radius of r_{HRS}, which locate nearby each other. When the average radius of the area where the n HRS filaments bundle is r_{HRS}' [Fig. 10(c)], Eq. (3) can be written as the relationship between the pad *I-V* current density (I_{HRS}^{P}) and APAFM current density (I_{HRS}^{A}) for the HRS. Here, it is assumed that the distance between the tiny filaments having a radius of r_{HRS} within the bundle is much smaller than the nominal tip moving distance between each measurement and d_{eff}. This suggests that the APAFM tip simultaneously contacts the n filaments or not at all at a given measurement. It was considered that the partial contact of some of the n filaments is not probable due to their small distance. This is the reason why the interaction area is assumed as having a diameter of $(d_{eff}-r_{HRS}')$ and not $(d_{eff}+r_{HRS}')$. If the area was assumed as having a diameter of $(d_{eff}+r_{HRS}')$, then the partial contact would have to be taken into consideration which renders the analysis too complicated to be analytically treated.

$$\frac{{r_{\mathrm{HRS}}}^2}{n(d_{\mathrm{eff}}-{r_{\mathrm{HRS}}}')^2}=\frac{{I_{\mathrm{HRS}}}^P}{{I_{\mathrm{HRS}}}^A}, \tag{3}$$

where n is the number of the filaments within the area with a radius of ${r_{\mathrm{HRS}}}'$.

Now, one more equation, [Eq. (4)], can be set if k' is expressed by using the APAFM data shown in Fig. 11 and the model shown in Figs. 10(a) and 10(c).

$$k'=\frac{{r_{\mathrm{LRS}}}^2\sigma_{\mathrm{LRS}}[{r_{\mathrm{LRS}}}^2/(d_{\mathrm{eff}}+r_{\mathrm{LRS}})^2]}{n{r_{\mathrm{HRS}}}^2\sigma_{\mathrm{HRS}}[{r'_{\mathrm{HRS}}}^2/(d_{\mathrm{eff}}-r'_{\mathrm{HRS}})^2]}. \tag{4}$$

Here, σ_{LRS} and σ_{HRS} are the specific conductivities of the filaments in LRS and HRS, respectively. The right-hand-side term in Eq. (4) can be understood as the ratio of the conductivities of the LRS (${r_{\mathrm{LRS}}}^2\sigma_{\mathrm{LRS}}$) and HRS ($n{r_{\mathrm{HRS}}}^2\sigma_{\mathrm{HRS}}$) multiplied by the probability that the tip actually touches the filament in one measurement $[{r_{\mathrm{LRS}}}^2/(d_{\mathrm{eff}}+r_{\mathrm{LRS}})^2$ for LRS and ${r'_{\mathrm{HRS}}}^2/(d_{\mathrm{eff}}-r'_{\mathrm{HRS}})^2$ for HRS] in APAFM. It was shown that k' is approximately 2.5. Furthermore, the current ratio from the pad *I-V* results of the LRS and HRS (R) can be formulated as Eq. (5) using the umber of conducting filaments in the LRS (M) and HRS (N) and their respective conductivities.

$$R=\frac{M}{N}\frac{{r_{\mathrm{LRS}}}^2\sigma_{\mathrm{LRS}}}{{r_{\mathrm{HRS}}}^2\sigma_{\mathrm{HRS}}}. \tag{5}$$

It was noted that R and (M/N) are 1300 and 40, respectively.

After combining Eqs. (1) and (3)–(5), r'_{HRS} was calculated to be $1.2r_{\mathrm{LRS}}$. This is a reasonable result considering the area ratio of the conducting spots from the LRS and HRS in the current mapping images using the APAFM (approximately same, data not shown). Therefore, it can be understood that the filament multiplication model, especially for the HRS film, during the APAFM measurements is a reasonable model and the change in the filaments during switching from the HRS to LRS can be modeled as shown; when a bias voltage (near V_{on}) is applied to a HRS TiO_2 film the current begins to flow through the tiny filaments that are already present in the film. Then the local heating near the filaments enhances the movement of point defects in that area and this forms a few more tiny nearby filaments. Finally, the enhanced current flow through all these bundled tiny filaments further enhances the movement of the point defects and these point defects may fill up the space between the tiny filaments and eventually form a filament with a bigger diameter and stronger correlation between the defects.

IV. CONCLUSION

In conclusion, the resistive switching behavior of atomic-layer-deposited TiO_2 thin films observed in macroscopic pad *I-V* measurements is closely related to conductive filament formation during voltage application. When the film changed from the initially highly insulating state to the state in which resistive switching was possible, the overall resistance fell off by approximately 10^6 times due to strong conducting filament formation (low resistance state). When the low-resistance state switched to the high-resistance state, the overall resistance increased by approximately 10^3 by the destruction of the strong filaments and formation of weaker and less conductive filaments (high-resistance state). The transition from the high-resistance state to the low-resistance state appears to occur via a mostly two-step process; a few more weak filaments are formed in the nearby area of preexisting weak filaments and they gather together to form stronger and better conducting filaments. During the switch back to the high-resistance state the stronger filaments appear to disassemble and only a few weak filaments remain. All switching events appear to have a close relationship with the heat production accompanying the current flow. However, resistive switching by formation and weakening of conductive filaments may not be used when sub-100-nm scale memory devices are fabricated with this material due to the relatively low area density of the filaments. Rather than switching via filament formation, where a resistance ratio of approximately 1000 was obtained, resistance switching of the area without filaments, where the resistance ratio of approximately 5 was obtained, should be utilized. The resistance change of the area without conducting filaments might have something to do with point defect generation but the exact mechanism is not clearly understood yet.

ACKNOWLEDGMENTS

The work was supported by the National Program for 0.1 Terabit NVM Devices and by the National Research Laboratories program of the Korean Ministry of Science and Technology. The collaboration between Seoul National University and Juelich groups was supported by the Alexander von Humboldt foundation. Two of the authors (C.S.H. and R.W.) acknowledge that.

[1] R. Waser, *Nanoelectronics and Information Technology* (Wiley-VCH, Weinheim, 2003), p. 527.
[2] I. G. Baek *et al.*, *Technical Digest—International Electron Devices Meeting*, San Francisco, CA, 12–14 December 2004 (unpublished).
[3] A. Asamitsu, Y. Tomioka, H. Kuwahara, and Y. Tokura, Nature (London) **388**, 50 (1997).
[4] A. Baikalov, Y. Q. Wang, B. Shen, B. Lorenz, S. Tsui, Y. Y. Sun, and Y. Y. Xue, Appl. Phys. Lett. **83**, 957 (2003).
[5] M. N. Kozicki, M. Mitkota, M. Park, M. Balakrishnan, and C. Gopalan, Superlattices Microstruct. **34**, 459 (2003).
[6] Y. C. Chen, C. F. Chen, C. T. Chen, J. Y. Yu, S. Wu, S. L. Lung, R. Liu, and C. Y. Lu, Tech. Dig. - Int. Electron Devices Meet. **2003**, 37.4.1.
[7] J. F. Gibbons and W. E. Beadle, Solid-State Electron. **7**, 785 (1964).
[8] F. Argall, Solid-State Electron. **11**, 535 (1968).
[9] Y. Watanabe, J. G. Bednorz, A. Bietsch, Ch. Gerber, D. Widmer, A. Beck, and S. J. Wind, Appl. Phys. Lett. **78**, 3738 (2001).
[10] G. Dearnaley, D. V. Morgan, and A. M. Stoneham, J. Non-Cryst. Solids **4**, 593 (1970).
[11] N. F. Mott, Rev. Mod. Phys. **40**, 677 (1968).
[12] K. Szot (private communication).
[13] S. K. Kim, W.-D. Kim, K.-M. Kim, C. S. Hwang, and J. Jeong, Appl. Phys. Lett. **85**, 4112 (2004).
[14] G. Dearnaley, A. M. Stoneham, and D. V. Morgan, Rep. Prog. Phys. **33**, 1129 (1970).
[15] K. Szot, W. Speier, R. Carius, U. Zastrow, and W. Beyer, Phys. Rev. Lett. **88**, 075508 (2002).
[16] T. B. Massalski, H. Okamoto, P. R. Subramanian, and L. Kacprzak, *Binary Alloy Phase Diagrams* (ASM International, Ohio, 1990), p. 2926.

[17]A. Grill, W. Kane, J. Viggiano, M. Brady, and R. Laibowitz, J. Mater. Res. **7**, 3260 (1992).
[18]J. Q. He, S. Regnery, C. L. Jia, L. Qin, F. Fitsilis, P. Ehrhart, R. Waser, K. Urban, and R. H. Wang, J. Appl. Phys. **92**, 7200 (2002).
[19]J. C. Shin, J. Park, C. S. Hwang, and H. J. Kim, J. Appl. Phys. **86**, 506 (1999).
[20]J. D. Baniecki, T. Shioga, K. Kurihara, and N. Kamehara, J. Appl. Phys. **94**, 6741 (2003).